Electronic Supporting Information

Parts of two papers (we recently published) are proposed to the readers, in order to prove that the existence of foreign 2D-adsorbed epi-layers on a growing crystal face is not a "hypothesis" but the logical consequence of ordered ab-sorption into the growth sectors, as evidenced by experimental measurements.

A. Calcite ($CaCO_3$) crystallizing in the presence of lithium ions

1) – The historical background

The influence of Li_+ ions on the crystal morphology of calcite became a matter of some interest twenty years ago, when: i)- Rajam and Mann found that the {00.1} platy form was added to the classic {10.4} cleavage rhombohedron growing in Li_+ doped aqueous solutions; ii)- Nefyodova et al. confirmed that {10.4} shaped seeds transform into crystals dominated by the {00.1} form in Li_+ bearing hydrothermal solutions. Both IR spectra and evaluation of the Li_+ segregation energy on the {00.1} form suggested that Li_+ cannot be absorbed within the growing calcite, but only randomly adsorbed in "…*lattice and not interstitial sites*…" on the {00.1} surfaces, so slowing down their advancement rate. No interpretation was given, at that time, on the growth mechanisms ruling this unusual morphological change (from kinked -K to flat -F character) of the {00.1} form.

2) – The "morphodrome" ($CaCO_3$, Li_+). The {00.1}, {01.8} *and* {10.4} *forms affected by the adsorption of Li_+ ions*

A practical way of representing the morphological changes of a crystal in the presence of a variable amount of an impurity, is to draw a *morphodrome*, i.e. a diagram with the impurity concentration (C_i) on the abscissa and the supersaturation, $\beta = (C-C_{eq})/C_{eq}$, with respect to the growing crystal, on the ordinate axis. In this way, the occurrence domain of the different morphologies can be drawn in a 2D space.

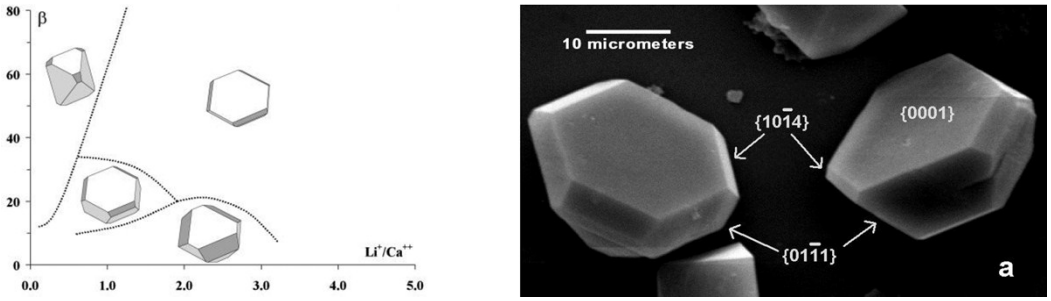

Fig. 1 *Morphodrome of calcite crystals nucleated and grown under varying initial [Li +]/[Ca^{2+}] concentration ratios and supersaturations. Different domains are associated to the most frequent observed habit. Figure reprinted with permission*

from "Morphology of calcite ($CaCO_3$) crystals growing from aqueous solutions in the presence of Li + ions. Surface behavior of the {0001} form" by L. Pastero, E. Costa, M. Bruno, M. Rubbo, G. Sgualdino, D. Aquilano; Crystal Growth & Design 4, issue 3 (2004), 485–490. Copyright C_2004, American Chemical Society.

Figure 1 shows that, when lithium is added to the aqueous solutions supersaturated with respect to calcite, the {00.1} and the {01.1} forms enter enriching the crystal morphology which was built up by the sole {10.4} form when formed from pure medium (under the same β value and $[Ca^{2+}]/[CO_3^{2-}]$ ratio). The importance of the {00.1} form increases when crystals nucleate and grow, in a steady state, in the presence of increasing amounts of lithium. Then, the crystal habit becomes more and more {00.1} platy starting from an initial $[Li^+]/[Ca^{2+}]$ concentration ratio equal to 0.01. From SEM and AFM observations it comes out that the {00.1} form shows layered surfaces within a wide range of supersaturations. A general ex-situ overview of crystals obtained at moderate β values ($4 < \beta < 37$) indicates that the {00.1} surfaces are populated by pseudo-hexagonal growth hillocks built by more or less periodic sequence of terraces and macrosteps (figures 2a,b).

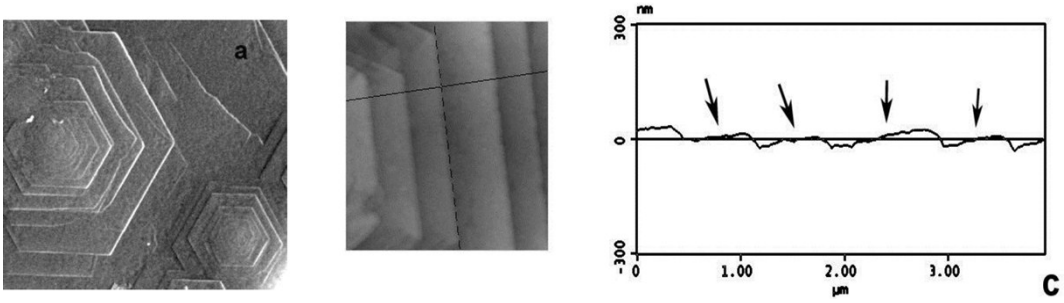

Fig. 2 *Surface structure of the {00.1} calcite form grown in the presence of lithium. (a) SEM image showing pseudo-hexagonal growth hillocks. Macrosteps run along the <100> directions. (b,c) AFM images of the profile of the terraces lying in between successive macrosteps showing small cobbles (arrows) and the wavy surface structure. Figure reprinted with permission from "Morphology of calcite (CaCO3) crystals growing from aqueous solutions in the presence of Li + ions. Surface behavior of the {0001} form" by L. Pastero, E. Costa, M. Bruno, M. Rubbo, G. Sgualdino, D. Aquilano; Crystal Growth & Design 4, issue 3 (2004), 485–490. Copyright 2004, American Chemical Society.*

Fig. 3 *Calcite crystal nucleated and grown from lithium bearing solution at high supersaturation values ($\beta \geq 37$): the {00.1} faces begin to roughen (left side). The slopes of the growth hillocks on the (00.1) faces (right side).*

Their mean thickness varies in between 5 and 35 nm, while the hillocks slope increases from 1° to 6.5° with increasing supersaturation. Hence it can be said that the kinetic behavior of {00.1} form is that of a F-form, independently of the step origin (2D nucleation or spiral growth). Moreover, from a deeper analysis of the profile of the terraces lying in between two successive macrosteps, it turns out that the terrace surfaces are not atomically flat. On the contrary, they are slowly wavy and populated by small cobbles whose height does not exceed a few nanometers (figure 5c). These cobbles behave as true obstacles for the spreading of the $d_{00.1}$ layers which slow down their advancement rate; this, in turn, generates the step bunching which is responsible of the macrostep occurrence.

Nevertheless, at low β values, the {00.1} form really behaves as a F form. But, as much as the supersaturation increases, both height and size of the terrace cobbles increases too, so slowing down the velocity of the macrosteps. A critical situation occurs when, at high β values, the cobbles height is able to compete with the macrosteps height, so hindering their flow. When this critical threshold is reached the inverse F → K transition takes place (see figure 3).

To clarify the effects induced by lithium on growing calcite crystals, one has to observe the {10.4} seeds, initially grown in pure medium and, successively, re-grown in a lithium bearing supersaturated solution: the layer growth starting from {00.1} surfaces can also propagate on contiguous {10.4} form and generates new {01.8} surfaces. Figures 4a,b illustrate two successive stages of this covering effect on a {10.4} seed. Figure 4a shows that once lithium is added to the mother solution new layers start to stabilize the {00.1} form and then continue spreading on the adjacent free surfaces following the symmetry imposed by the triad [001] axis.

Figure 4b shows a successive stage of the covering which stopped just before the initial rhombohedron was entirely encompassed. It is worth also outlining that the <-441> edges of the original seed were replaced (during growth) by small rectangular shaped {01.8} surfaces. Moreover, the macroscopically stepped profile which characterizes the {01.8} surfaces of the natural samples (figure 5a) does no longer appear in crystals grown in the presence of lithium; on the contrary, the {01.8} surfaces illustrated in figure 4 are smoothed and look like those of the adjacent {10.4} and {00.1} flat forms. We may invoke also in this case the role of the 2D epitaxy as the modifier of the character of {01.8} surfaces (from S to F).

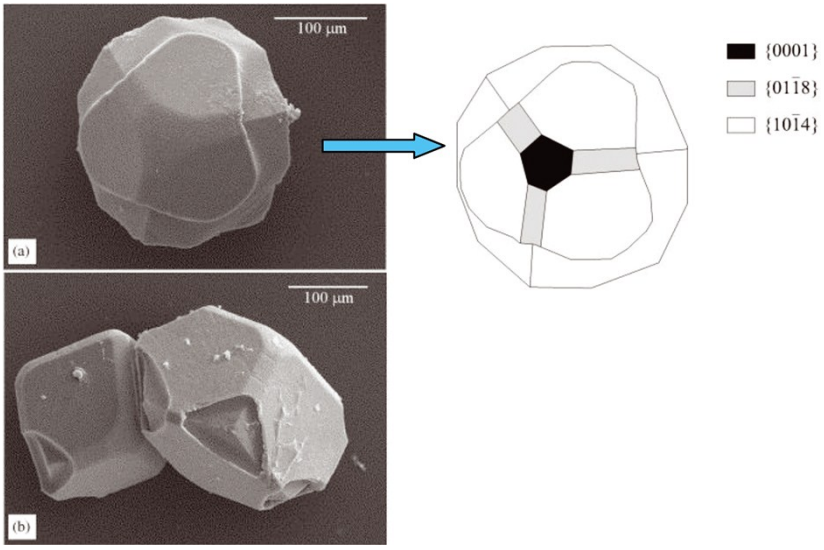

Fig. 4 (a,b) *The morphology changes induced on the {10.4} seeds of calcite by the presence of Li + ions in the mother solution. The new {00.1} and {01.8} surfaces are smoothed and look like those of the adjacent {10.4} flat form.*

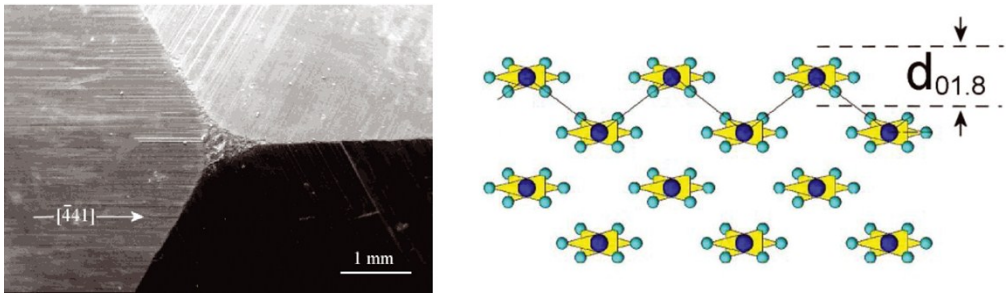

Fig. 5 *(Left side): Striations that characterize the <-441> stepped profile of {01.8} surfaces of natural samples. (Right side): The character of this form is stepped since no bond exists between the <-441> PBCs (viewed up-down) within a d018 slice. Figures 3, 4 and 5 have been adapted with permission from "2D-epitaxy of lithium carbonate inducing growth*

mechanism transitions on {00.1}-K and {01.8}-S forms of calcite crystals" by L. Pastero, D. Aquilano, E. Costa, M. Rubbo; Journal of Crystal Growth 275, issue 1–2 (2005), e-1625 e-1630. Copyright C_2005, Elsevier.

As a matter of fact, new lattice coincidences are found (Table 1) between Li_2CO_3 and calcite when comparing the 2D mesh of the {01.8} calcite surfaces with those of the {001} and {100} forms of the Li_2CO_3 structure:
From Table 1 one can see the excellent 2D-coincidences between both the $\{001\}_{zabuyelite}$ and $\{100\}_{zabuyelite}$ forms and the $\{01.8\}_{calcite}$. It should be also remembered that $\{001\}_{zab}$ is a F form while $\{100\}_{zab}$ is a S one, as it ensues from the PBC analysis. Further, $\{001\}_{zab}$ is the most important form entering the equilibrium shape of the crystal, whilst the $\{100\}_{zab}$ is excluded owing to the high value of its surface energy . Then $\{001\}_{zab}$ seems to be favored to make epi-layers which should change the character (S→F) of the $\{01.8\}_{calcite}$. Concerning the fit of d_{002} and d_{200} zabuyelite layers with the $d_{01.8}$ of calcite, the related contributions to the formation of anomalous mixed crystals will be discussed later on.

Table 1 *Coincidences at the {01.8}calcite/{001}zabuyelite and {01.8}calcite/{100}zabuyelite interfaces.*

	Calcite {01.8} *host*	*Zabuyelite* {001} *guest*	Misfit(%)	obliquity
2D cell vectors and length (Å)	$\|[010]\| = 4.989$	$\|[010]\| = 4.972$	+0.34	0°
	$2/3\times\|[010]\| = 25.66$	$3\times\|[100]\| = 25.17$	+1.95	
Layer thickness (Å)	$d_{01.8} = 1.9125$	$d_{002} = 2.81229$	- 47.04	
	Calcite {01.8} *host*	*Zabuyelite* {100} *guest*		
2D cell vectors and length (Å)	$\|[010]\| = 4.989$	$\|[010]\| = 4.972$	+0.34	0°
	$1/3\times\|[48\bar{1}]\| = 12.83$	$2\times\|[001]\| = 12.42$	+3.30	
Layer thickness (Å)	$2\times d_{01.8} = 3.825$	$d_{200} = 3.79327$	+0.836	

Table 2 *Lattice coincidences at the {00.1}calcite/{001}zabuyelite interface.*

	Calcite{00.1 }host	Zabuyelite {001} guest	Misfit(%)	obliquity
2D cell vectors and length (Å)	$\|[210]\| = 8.64$	$\|[100]\| = 8.359$	+3.3	0°
	$\|[010]\| = 4.989$	$\|[010]\| = 4.972$	+0.34	
Layer thickness (Å)	$d_{00.6} = 2.843$	$d_{002} = 2.812$	+1.1	

Aiming at explaining the lithium effect on the appearance of both the new {00.1} and {01.8} forms of calcite, we will adopt the interpretative path proposed by the Kern's school. At first, we will reasonably concentrate our attention on the epitaxy model (geometric and structural) of the adsorbed (001)-Li_2CO_3 layers on the (00.1)-$CaCO_3$ substrate.

3) – The epitaxial model of the interface between (001)-Li_2CO_3 (zabuyelite) and the substrate (00.1)-$CaCO_3$ (calcite)

The space group of calcite is R3c and its parameters (hexagonal frame, in Å), are: $a_o = 4.989$, and $c_o = 17.06$, while Li_2CO_3, at ambient conditions, is monoclinic (C2/c), with $a_o = 8.39$, $b_o = 5.00$, $c_o = 6.21$, $\beta = 114.50°$. Comparing these structures, viewed along their [010] directions, one can see that their geometrical misfits are very low (Table 2).

i) This means that the *geometrical conditions* for epitaxy between the (00.1) face of calcite crystal and the d_{002} layers of lithium carbonate are largely fulfilled.

ii) Concerning the *structure of the epitaxial d_{002} layer of Li_2CO_3* it is worth outlining that the outmost Li^+ ions, which should face the outmost (00.1) layer of calcite, form a perfect 2D hexagonal lattice, as it can be seen onto a projection of the Li_2CO_3 structure normal to the 001 plane. Entering into details, Li^+ ions lie in the origin of the 2D space group *p6m*, the lattice vector corresponding to $b_{Li_2CO_3} = 4.972$ Å . This lattice coincides (misfit of 0.2%) with that built by the vacant sites resulting from the second restructured layer of calcite (00.1). In other words and remembering the reconstruction of {111} NaCl surfaces , one can say that, if the outmost calcite layer contains only the 25% of CO_3^{2-} ions, in the second last one the 75% of available sites will be occupied by Ca^{2+} ions while the Li^+ ions could fill the remaining ones. Hence a d_{002} layer of Li_2CO_3 can be adsorbed on the $(00.1)_{calcite}$ face. Within this layer, three PBC's develop: the strongest one is the [010] PBC, while the two others are the < -110> PBC's.
The adsorbed layer behaves as a 2D crystal which imposes its own PBC's to the underlying face . In our peculiar case the strong [010] PBC of the Li_2CO_3 adsorbed layer runs along the same direction of the [010] steps we observed and described above; moreover, owing to the three-fold symmetry of the (00.1) face of calcite, the adsorbed impurity shall impose three strong PBC's to the face which, in turn, transforms its character from kinked to flat (K→F transition).

4) – The third condition to be fulfilled to get an "anomalous Calcite/Zabuyelite mixed crystal"

Another geometric concordance, even not necessary for the epitaxy to occur, is that found between the thickness of the epitaxial layers of both structures. From systematic extinction rules, the thicknesses allowed (in Å) are $d_{00.6} = 2.843$ Å and $d_{002} = 2.812$ Å for calcite and Li_2CO_3, respectively: then, the relative misfit does not reach +1.1%.

Table 3 *Lattice coincidences at the {10.4}calcite/{111}zabuyelite interface.*

	Calcite {10.4 }host	Zabuyelite {111} guest	Misfit(%)	obliquity
2D cell vectors and length (Å)	$1/3 \times \lvert[42\bar{1}]\rvert = 8.11$	$\lvert[0\bar{1}1]\rvert = 7.9436$	+2.09	2.34°
	$\lvert[020]\rvert = 9.9792$	$\lvert[\bar{1}10]\rvert = 9.7266$	+2.6	
Layer thickness (Å)	$d_{10.4} = 3.043$	$d_{111} = 3.0311$	+0.39	

Thus, the parametric coincidences (in the three space directions) between the absorbed and the adsorbing crystal phases, should be fulfilled in order an *anomalous Calcite/Zabuyelite mixed crystal* to be formed. To verify this hypothesis, i.e. to investigate whether and how lithium can be absorbed into the calcite lattice, integrated characterization techniques, such as ICP, SEM, AFM, XRPD, cathodoluminescence (CL) and EPR, have been applied to a wide population of calcite single crystals grown from solution and gels.

4.1.) – CL measurements

These measurements take advantage of the incompatibility between the structure of Li-carbonate and the Mn^{2+} ions (present as impurity in the gel matrix) captured in it. Furthermore, it is well known that Mn^{2+} capture in carbonates shows marked CL effect since Mn-depleted sectors are frankly darker than the richer ones. From CL measurements one can argue the existence of irregular stacking sequences of Mn^{2+} rich and Mn^{2+} depleted layers within the {00.1} growth sectors of calcite and this proves, indirectly, that ***lithium has been buried during growth*** in the Mn^{2+} depleted layers.

4.2.) – XRPD measurements

The 10.4 is the highest diffraction peak of calcite. In pure $CaCO_3$ samples, the highest intensity elementary curve among the ones resulting from the decomposition (figure 6a), is located at $d_{10.4} = 3.043$ Å . With increasing Li^+ amount in the growth solution, the maximum intensity progressively shifts toward lower inter-planar spacing, that is at $d_{10.4} = 3.031$ Å and $d_{10.4} = 3.028$ Å when $Li^+/Ca^{2+} = 5$ and 25, respectively (figure 6b,c). Hence the dispersion of the maximum is not symmetric around the averaged value of the peak $<d_{10.4}> = 3.035$ Å .

It is worth noting that the 111 peak of pure Li_2CO_3 crystals occurs at $d_{111} = 3.0311$ Å and that, consequently, the presence of mixed $CaCO_3$-Li_2CO_3 layers in the {10.4 } growth sectors of calcite should affect the position of the maximum corresponding to the $d_{10.4}$ peak. As a matter of fact, a new relationship can be obtained at the $\{10.4\}_{calcite}/\{111\}_{zabuyelite}$ epitaxial interface, as illustrated in the following Table 3 and in figure 7.

From figure 7 it follows that an elementary $d_{zabuyelite\ 111}$ slice can only grow through 1D-nucleation of uncorrelated [110] chains and then their adsorption on the {10.4 } form of calcite is less favored with respect to that of 2D-nuclei of zabuyelite (of thickness d_{002}) on the $\{00.1\}_{calcite}$ pinacoid. Nevertheless, if the adsorption occurs, 1D zabuyelite chains can be easily buried within the {10.4} growth sectors by new freshly created calcite layers, owing to the quasi perfect coincidence between the layers thicknesses of the two crystals. This seems to be the most reasonable way of explaining the progressive shift of the highest intensity component of the 10.4 diffraction peak (and hence of the lowering of the $d_{10.4}$ value) of our crystals, with the increasing lithium concentration in the growth solution.

The 00.6 diffraction peak is an important one, its intensity being 73/100 of the 10.4 reference peak. Its decomposition (figure 6d,e,f) yields a unique averaged value $<d_{00.6}> = 2.847$ Å , corresponding to $c_0 = 17.080$ Å which is very close to the value of 17.073Å calculated from the overall XRPD spectra in non-lithium bearing calcite crystals. But, when the Li^+ amount increases in the growth solution, the peak shape dramatically changes and the spacing coming out from the decomposition spreads over a $<d_{00.6}>$ interval of 0.169 Å , resulting in a fairly symmetrical peak dispersion around $<d_{00.6}>$.

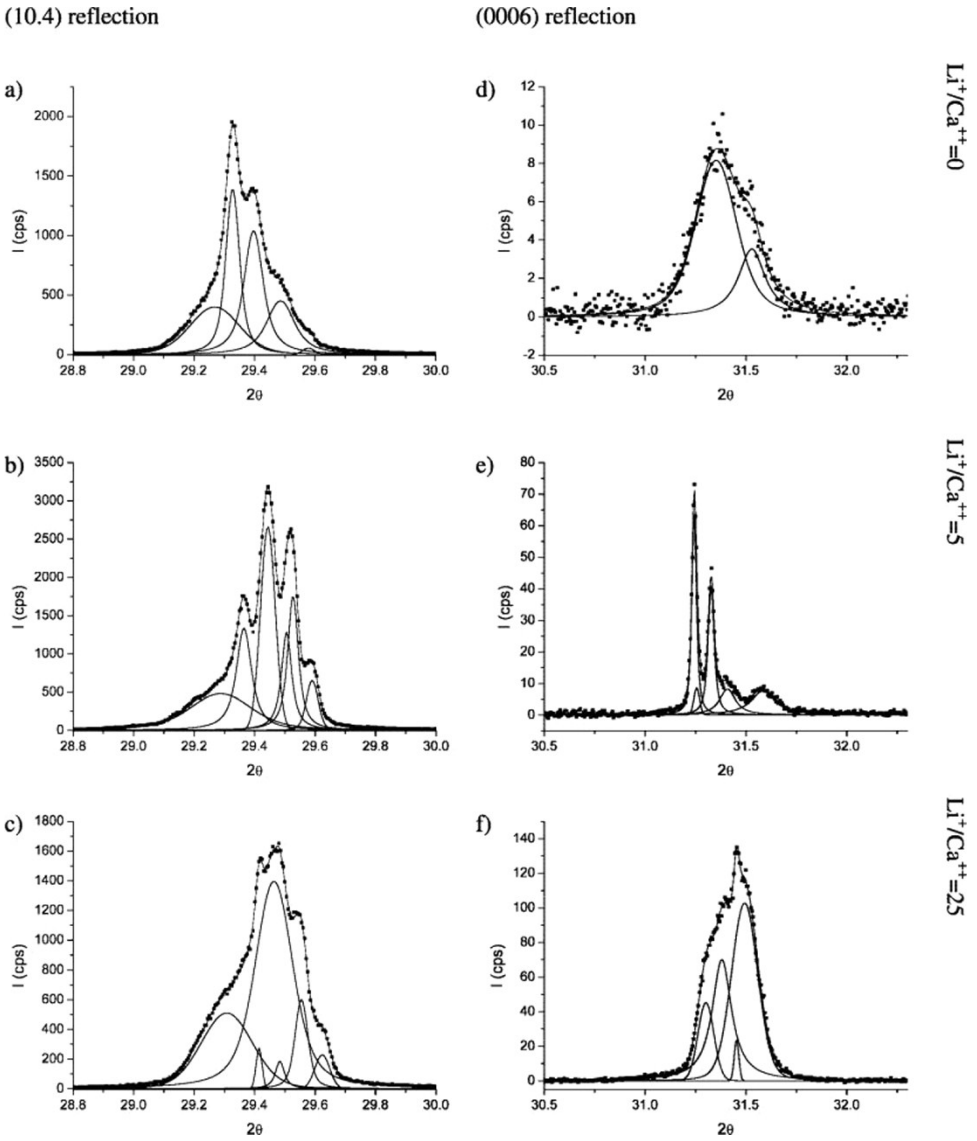

Fig. 6 *In pure $CaCO_3$ samples (a) the highest elementary curve is located at $d_{10.4}$ = 3.043 Å . With increasing Li+ amount in the growth solution, the maximum progressively shifts toward lower spacing, that is at $d_{10.4}$ = 3.031 Å and $d_{10.4}$ = 3.028 Å when $Li+/Ca^{2+}$ = 5 and 25, respectively (b,c). This is due to the overlapping of the Li_2CO_3 layers of thickness d_{111} = 3.0311Å in the {10.4 } growth sectors of calcite. An analogous behavior is illustrated for the 00.6 peak of calcite (d-f) which is strongly affected by the overlapping of the absorbed Li_2CO_3 crystal layers of thickness $d_{00.2}$.*

All this further proves that:
i) Li_+ ions are absorbed in calcite taking the structure of zabuyelite layers and mainly locate in the {00.1} growth sectors of calcite, so perturbing the ordered stacking of its $d_{00.6}$ layers. This should induce zones of compression and distension that reflect in the spreading of the parameter c_0 from 16.985 to 17.154 Å (being $c_{0,}$ in pure calcite crystals, equal to 17.073 Å).
ii) Another growth sector affected by lithium absorption, even if to a lesser extent, is that of the {10.4} rhombohedron. This is not surprising, since we already observed that pure calcite seeds, originally limited only by the {10.4} form, are encompassed by thick growth layers which start to grow from the new generated {00.1} form, when lithium is added to the growth solution (see the preceding figure 4).

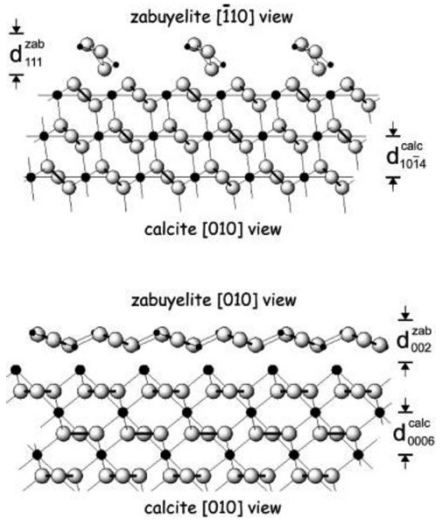

Fig.7 *Projections of calcite and Li2CO3 (zabuyelite). Large and small spheres represent calcium and lithium atoms, respectively*

(Top): The structure of the {10.4}calcite/{111}zabuyelite interface: the {111}form of zabuyelite is a stepped one, since any bond can be found among adjacent [110] PBCs of zabuyelite within a d111 slice.
(Bottom): The structure of the {00.1}calcite/{001}zabuyelite interface. The thickness of the elementary layers are near the same in both structures, d00.6 (calcite) being practically equal to d002 (Li2CO3). Figures 6 and 7 are reprinted with permission from: "CaCO3 (calcite)/ Li2CO3 (zabuyelite) anomalous mixed crystals. Sector zoning and growth mechanisms" by L. Pastero, D. Aquilano; Crystal Growth & Design 8, issue 9 (2008), 3451–3460. Copyright C_2008, American Chemical Society.

5) – A first tentative conclusion

Summing up:
i) The incorporation of lithium into calcite crystals does not randomly occur, but needs an epitaxial mediation. This means that 2D coincidence lattices between lithium and calcium carbonates (so different in symmetry, but so close as concerns the structural packing) are not limited to a geometrical meaning but represent the necessary condition for lithium to be incorporated through the epitaxial adsorption of PBCs (1D) or islands (2D).
ii) Adsorption is followed by the absorption into growing calcite crystals, owing to the strong similarity between the thickness of the adsorbed elementary layers and those of the underlying reactive substrate.
iii) Thus, the anomalous mixed crystal originates thanks to a selective mechanism, since the probability of lithium entering the calcite lattice varies from {00.1} to {10.4} growth sectors, the first one being largely favored, as it ensues from the contrast shown by cathodoluminescence imaging.
iv) On this ground, the anomalous calcite/zabuyelite mixed crystals, in the sense of Johnsen and Neuhaus, are not homogeneous, as proved by the cathodoluminescence and the different spreading of the 00.1 and 10.4 XRPD peaks.

B. Halite (NaCl) crystallizing in the presence of formamide (H-CO-NH_2)

1) - {100} → {111} morphological change in NaCl crystals growing from aqueous solutions in the presence of formamide. The literature data.

The following Figure 1. S.I. (top) was originally drawn by Bienfait, Boistelle and Kern, in "Adsorption et Croissance Cristalline- Colloques Internationaux du CNRS", 1952, Ed. CNRS-Paris. Figure 1. S.I. (bottom) shows the morphology of NaCl grown from pure aqueous solution and from water+formamide (20%) solution evaporating at 25 °C.

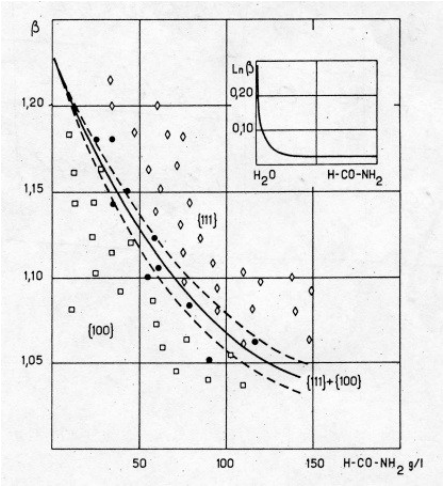

Fig.1S.I.

(top)- Morphodrome of NaCl crystals grown from aqueous solutions in the presence of formamide (concentrations on the x-axis); on the y-axis, the initial supersaturation of the solution with respect to NaCl. In the inset: the morphodrome represents the situation comprised between the limiting cases of pure water and pure formamide solutions.

(bottom, from left to right): {100} form from pure aqueous solution; {100}+{111} forms from aqueous solution containing 20% of formamide, obtained by evaporation at 25°C; a macrostep spreading on the {111} form (detail of the preceding case); only the {111} form occurs when crystals grow from pure formamide solutions.

Reprinted and adapted with permission from: "Selective adsorption/absortion of formamide in NaCl crystals growing from solution" by L. Pastero, D. Aquilano, M. Moret; Crystal Growth &Design 12, issue 5 (2012) 2306-2314. Copyright ©2012, American Chemical Society.

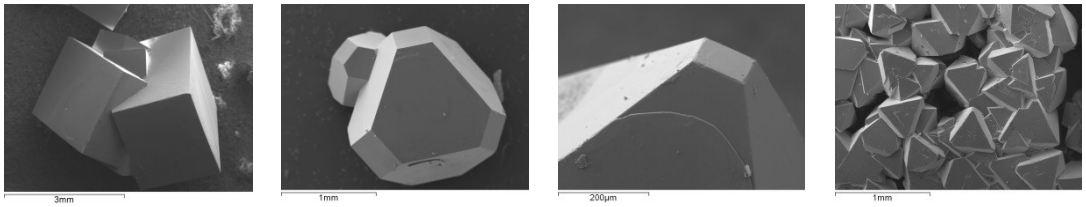

In the belief that such a dramatic change of morphology might be hardly interpreted in the light of the sole interactions between isolated molecules and the crystal surface, we investigated the structure of formamide, hoping to find if any cooperative effect (such as the epitaxial relationships) can set up between the crystal structures of NaCl (host phase) and formamide (guest phase). To do this, we started from the structure of formamide.

2) - The structure of formamide

At the temperature of 223 K, formamide is monoclinic (S.G. $P2_1/n$), its lattice parameters being: a_0=3.69 Å, b_0=9.18 Å, c_0=6.87 Å, β=98°. Its structure can be viewed as made by adjacent sheets of molecules which are parallel to the 101 plane and separated by the distance d_{101} which reaches the value of 3.09 Å at 0°C, just below the melting point (+2°C), at room pressure (see table 1. S.I.). Within the sheets, pairs of molecules associate to form almost coplanar dimers. Puckering of the sheets results from the tilt of the bimolecular units relative to one another. N-H···O bonds of two types cross-link the chains forming each sheet: H-bonds (α), 2.93 Å nm long, link monomers to form dimers, while H-bonds (β), 2.88 Å nm long, link

dimers together. In the light of the Hartman-Perdok theory, one can say that two PBCs run within the layers of thickness d_{101}: the PBC [010], developing along the screw A_2 axis through α -bonds and the PBC $[11\bar{1}]$ made by β-bonds. Remembering that no H-bonds can be found outside the d_{101} layers, one can consider the (101) pinacoid as the most important F form of the crystal and then that the theoretical crystal habit (at least from vapor phase) should be {101} platy. This is the main reason why we chose the 101 plane as the best candidate for a hypothetical epitaxy between a d_{101} layer of formamide and the growing NaCl-{111} form.

	NaCl {111}-*Host*	*formamide* {101}- *Guest*	misfit %	obliquity
2D cell vectors (Å)	$\lvert[11\bar{2}]\rvert = 13.81$	$3/2\lvert[010]\rvert = 13.84959$	-0.286	0°
	$\lvert[1\bar{1}0]\rvert = 7.976$	$\lvert[10\bar{1}]\rvert = 8.16682$	-2.392	
layer thickness (Å)	$d_{111} = 3.25$	$d_{101} = 3.0947$	+ 4.778	-----

Table 1 S.I. *Coincidences at the* $\{111\}_{NaCl}/\{101\}_{formamide}$ *interface. Structural data are extrapolated at T= 0°C, from formamide structures determined at 90 K, 108K and 223 K, respectively*

From Table 1 one can be aware of a striking 2D-lattice coincidence that may set up at the $\{111\}_{NaCl}$ / $\{101\}_{formamide}$ interface and between the thickness of the elementary d_{111}^{NaCl} and $d_{101}^{formamide}$ layers. All this means that it is worth searching for prove the existence of NaCl / formamide anomalous mixed crystals.

3) - The {100} → {111} NaCl morphological change due to formamide ad-sorption and its selective ab-sorption in the bulk of the NaCl lattice

Starting from the experience acquired in the formation of the calcite/zabuyelite anomalous mixed crystals, we did not confine our attention to the morphology of the NaCl crystals grown in the presence of formamide, but investigated also their bulk structure, in order to find if the adsorption → absorption mechanism would also occur in this new case. Fig.2 S.I. shows the XRPD spectra recorded on different populations of NaCl crystals obtained at different crystallization temperature (T_c) and from solutions containing different concentrations of formamide (C_f). Two main (2θ) intervals, corresponding to the d_{111} and d_{002} equidistances of the NaCl crystal are worthy of consideration.

(a) $27° \leq 2\theta \leq 28°$ → the coexistence of 111_{NaCl} and the $101_{formamide}$ reflections

$i_{(111)}$ A saturated (T_s=95°C) NaCl aqueous solution (C_f =20%) was cooled, under a gradient of 20°/h, at = -5°C. XRPD spectra were carried out at T=-5°C as well, on a large population of un-grinded as grown {111} platy shaped crystals. Fig.12a, left side shows two diffraction peaks. The first one, at lower 2θ values, corresponds to the integrated $\lambda_{K\alpha 1}$ and $\lambda_{K\alpha 2}$ contributions of the reflection $< d_{111}^{NaCl} >$=3.2593 Å. The second one, i.e. the low intensity peak at 2θ =27.695, *cannot be indexed as a NaCl reflection* but as the $d_{101}^{formamide}$ = 3.2209 Å (using the averaged $\lambda_{K\alpha 1,2}$ =1.54178 Å). This $d_{101}^{formamide}$ value is slightly higher (+4.07%) than the calculated one (3.0947 Å) by extrapolation of structural data of the pure formamide. This means that NaCl crystals were able to capture formamide in their bulk during growth (either through fluid inclusions or by absorption of ordered d_{101} layers, or both). Since these spectra were obtained at T=-5°C, where formamide is necessarily crystallized, other measurements must be made at T ≥ +2°C, i.e. beyond its melting point. Therefore, all the experiments described in the following were performed by evaporating a solution (T_{ev}=30°C) and the corresponding XRPD spectra were carried out at T=+25°C.

ii$_{(111)}$ NaCl crystals formed from a water/formamide solution(C_f =20%). Their morphology is made by dominating {100} and small {111} forms. The 111_{NaCl} peak is weakly asymmetric (due to the $\lambda_{K\alpha 1}$ and $\lambda_{K\alpha 2}$ components) and yields $<d_{111}^{NaCl}>$=3.2604 Å. No other peak occurs in the observed 2θ range. (Fig.2b, left side) The small increase (+0.033%) of the d_{111}^{NaCl} value is not surprising, owing to the increased temperature of measurement (from −5 to +25°C). However, no *ad*-sorbed $d_{101}^{formamide}$ layers are found to be orderly *ab*-sorbed in the growing NaCl crystal.

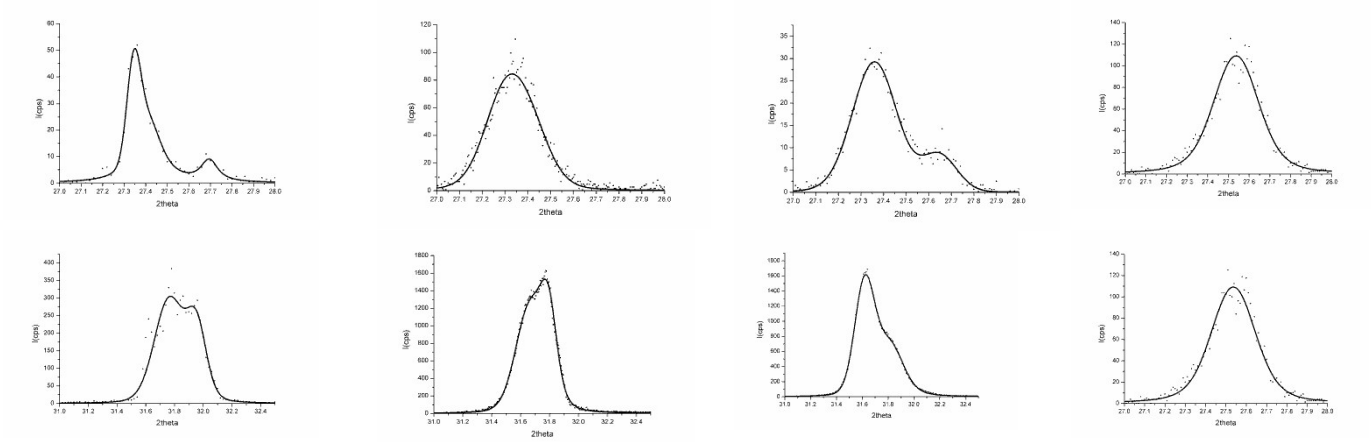

Fig.2 S.I. a: XRPD spectra performed at T= −5°C on crystals obtained at T_{cr}= −5°C from a NaCl aqueous solution(T_s=95°C; C_f =20%) cooled under a gradient of 20°/h. Top: 111_{NaCl} peak (lower angle) + $101_{formamide}$ peak (higher angle).

Bottom: 002_{NaCl} peak

b: spectra performed at T=25°C on crystals obtained by evaporation at T_{cr} = 30°C from a NaCl aqueous solution (initial C_f =20%).

Top: asymmetric 111_{NaCl} peak (lower angle).

Bottom: 002_{NaCl} peak

c: spectra performed at T=25°C on crystals obtained by evaporation at T_{cr} = 30°C from a NaCl aqueous solution (initial C_f =60%).

Top: asymmetric 111_{NaCl} peak (lower angle).

Bottom: 002_{NaCl} peak

d: spectra performed at T=25°C on crystals obtained by evaporation at T_{cr} = 30°C from a NaCl pure formamide solution (C_f =100%). Top: 111_{NaCl} peak.

Bottom: 002_{NaCl} peak

Reprinted and adapted with permission from: "Selective adsorption/absortion of formamide in NaCl crystals growing from solution" by L. Pastero, D. Aquilano, M. Moret; Crystal Growth &Design 12, issue 5 (2012) 2306-2314. Copyright ©2012, American Chemical Society.

iii$_{(111)}$ NaCl crystals were obtained from a new water/formamide solution (C_f =60%). Their morphology is now made by dominating {111} and small {100} forms. The full width at mean height (FWMH) of the 111_{NaCl} peak ($<d_{111}^{NaCl}>$ =3.2596 Å) increases with respect to the preceding case. A satellite peak occurs at 2θ =27.650 and corresponds to $d_{101}^{formamide}$ = 3.226 Å (Fig.12c, left side). Any effect of crystallization of formamide fluid inclusions must be excluded since both the crystallization and recording temperatures were largely higher than the melting point of formamide. Then, when the concentration of formamide competes with that of water, the $d_{101}^{formamide}$ layers are not only epitaxially adsorbed on the 111_{NaCl} surface but also buried in the growing crystal.

iv $_{(111)}$ The just mentioned conclusion is spectacularly confirmed by NaCl crystals obtained from pure formamide solution. The only form is the {111} octahedron. XRPD spectra yielded *a unique and symmetric peak which locates in between the 111_{NaCl} and the $101_{formamide}$ peaks*.(Fig.2d, left side) Thus, as a first approximation, $d_{111_{NaCl}}^{101_{formamide}}$ = 3.2393 Å.

(b) 31°≤ 2θ ≤ 32.5° → the $002_{(NaCl)}$ reflection

The behaviour of the $002_{(NaCl)}$ reflection is rather different with respect to the preceding one. In the $31° \leq 2\theta \leq 32.5°$ interval there is no risk of overlapping between the $002_{(NaCl)}$ peak and formamide reflections. Nevertheless both the d_{002}^{NaCl} value and the corresponding peak profile are affected by the formamide layers absorbed in the crystal within the {111} growth sectors. In the following we will illustrate the behaviour of the $002_{(NaCl)}$ peak, analogous of the just described situations (from $\mathbf{i}_{111}$ to iv_{111}):

$\mathbf{i}_{(002)}$ C_f =20%; $T_{crystallization}$ = -5°C; XRPD spectra were performed at T=-5°C, as in **$\mathbf{i}_{(111)}$**. A large peak is obtained, its complex profile being composed by three different contributions (Fig.2a,right side): a low angle component due to d_{002}^{NaCl} =2.827 Å, a medium angle component located at d_{002}^{NaCl} =2.8137 Å and a high angle component at d_{002}^{NaCl} =2.7974 Å. The averaged value of these spacing locates at $d_{002}^{NaCl}{}_{\text{averaged}}$ = 2.8127 Å which is – 0.35% lower that the corresponding value calculated from the reflection $<d_{111}^{NaCl}>$=3.2593 Å observed in $\mathbf{i}_{111}$. This is not surprising if one remembers that the {111} platy shape of the crystals obtained in this case favors the dispersion of the d_{002}^{NaCl} spacing owing to the varying amount of formamide captured within the d_{111}^{NaCl} layers in the +95°C → -5°C growth interval.

$\mathbf{ii}_{(002)}$ C_f =20%, T_{ev} = 30°C → The 002 peak profile is asymmetric (Fig. 2b,right side): from the lower angle component the averaged value ($\lambda_{K\alpha 1,2}$) results to be $<d_{001}>_{\text{lower angle}}$ = 5.6515 Å which only differs by –0.033% from the calculated $<d_{001}>$ = 5.6534 Å obtained from the measured $<d_{111}>$ =3.2604 Å (as it can be seen in ii_{111}). Further, the averaged value of the higher angle component of the asymmetric peak locates at $<d_{001}>_{\text{higher angle}}$ = 5.6288 Å, so showing that within the same crystal population there are two generations of $<d_{001}>$ equidistances, which are differently affected by the capture of d_{101} ordered layers of formamide. In this case, the split of $<d_{001}>$ = ($<d_{001}>_{lower\ angle}$ − $<d_{001}>_{higher\ angle}$) is 0.0227Å

$\mathbf{iii}_{(002)}$ C_f =60%, T_{ev} = 30°C → The 002 peak profile maintains asymmetric, but its shape changes, due to the displacement of its two components (Fig.12c,right side). From measurement: $<d_{001}>_{lower\ angle}$ = 5.6603 Å while $<d_{001}>_{higher\ angle}$ = 5.6262 Å → the split reaches 0.0341 Å .The variation in the splitting of the two components of the 002_{NaCl} peak confirms that the increase of the formamide concentration in solution enhances as well the relative importance of the {111} surfaces and, ultimately, of the {111} growth sectors which are affected by the presence of absorbed layers of formamide. This, in turn, influences the value of the $<d_{001}>$ equidistance, according to relative portion of the {111} growth sectors which are intersected by the 001 lattice planes.

$\mathbf{iv}_{(002)}$ C_f =100%, T_{ev} = 30°C → As for the 111 peak, the shape of the 002 reflection, located at $<d_{001}>$ = 5.6238 Å becomes symmetric (Fig.12d,right side). Compared with the corresponding $<d_{001}>$ = 5.6106 Å value, calculated from the measured 111 peak obtained under the same growth condition (see $\mathbf{iv}_{111}$), its deviation does not exceed –0.23%.

Summing up, from the detailed XRPD spectra carried out on the as grown NaCl crystals obtained in the presence of varying concentrations of formamide and having considered the related changes of their growth morphology, one can say:
a) – formamide easily adsorbs on the $\{111\}_{NaCl}$ surfaces, so generating the morphological transition: {100}→ {100} + {111}. This change was attributed to the adsorption of isolated formamide molecules on the {111} surfaces. Through the observation of macrostep spreading on the {111} surfaces we found that formamide induces a K → F change in the character of the {111} form and, searching for lattice coincidences, we put forward the hypothesis of a 2D epitaxy setting up between the $101_{formamide}$ lattice planes and the $\{111\}_{NaCl}$ surfaces. Hence, the most reasonable model of formamide adsorption is not "random-molecular" but "2D-epitaxial islands".
b) – The thickness of the epitaxially adsorbed $d_{101}^{formamide}$ layers fits very well ($\Delta d << 5\%$) with the height of the elementary d_{111} steps of NaCl crystals. Hence, one can reasonably suppose that the adsorbed layers can be easily buried in the $\{111\}_{NaCl}$ sectors during growth.
c) – XRPD spectra carried out on as grown NaCl crystal populations, under different temperature of crystallization and formamide concentration (C_f) in aqueous solutions, evidenced that the 111 and 002 reflections of NaCl are profoundly and differently modified according to both temperature and (C_f) value, the main factor of change being the relative size of the "formamide contaminated" $\{111\}_{NaCl}$ growth sectors. This unambiguously proves our hypothesis put forward in (*b*).
d) – When NaCl crystals nucleate and grow from pure formamide solution, XRPD spectra indicate that only the {111} growth sectors exist in the crystals.

Figure ESI_1: The alternative coincidence cell between {111}- NaF (left side) and {101}- formamide (right side), as illustrated in Table ESI_1a

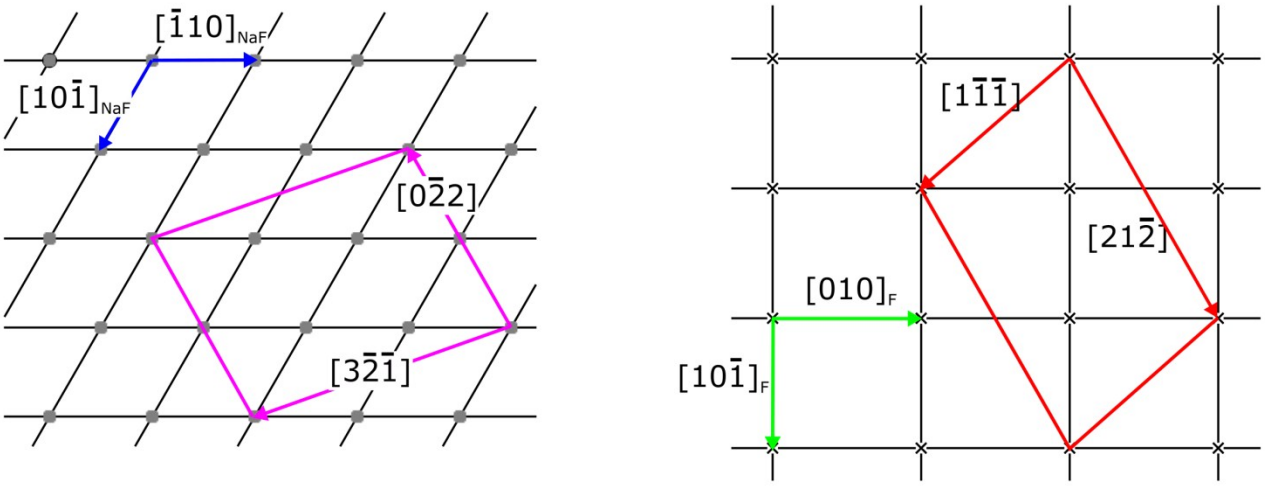

Table ESI_1. The coincidence lattices between formamide and the alkali halides in the "NaF mode" (a comparison between *LiF, NaF* and *LiCl*)

	Host crystal	**Guest crystal**	**Misfit *m* (%)**	**Notes**
	LiF {111}	**formamide {101}**		
2D-cell vectors	$[2\bar{3}1]$ = 15.0675 $[2\bar{1}\bar{1}]$ = 9.8640	2×$[10\bar{1}]$= 16.165 $[11\bar{1}]$= 12.296	+7.28 +24.66	Low linear misfit Very high linear misfit
2D-cell Area	**112.35**	149.804	**+33.33**	Very high area misfit
Layer thickness (Å)	4×d_{111} = 9.299	3×d_{101} = 9.399	**+1.065**	Good compatibility for 2D absorption
	NaF {111}	**formamide {101}**		
2D-cell vectors	$[2\bar{3}1]$ = 17.337 $[2\bar{1}\bar{1}]$ = 11.350	2×$[10\bar{1}]$= 16.165 $[11\bar{1}]$= 12.296	–7.25 +8.34	Low and opposite linear misfits
2D-cell Area	148.754	149.804	**+ 0.70**	Very low area misfit
Layer thickness	5×d_{111} = 13.38	4×d_{101} = 12.53	– 6.74	Low compatibility for 2D

(Å)				absorption
	LiCl {111}	**formamide {101}**		
2D-cell vectors	$[2\bar{3}1]$ = 19.232 $[2\bar{1}\bar{1}]$ = 12.590	$2\times[10\bar{1}]$= 16.165 $[11\bar{1}]$= 12.296	**–18.97** –2.39	Very high linear misfit Low linear misfit
2D-cell Area	183.04	149.804	**–22.18**	Very high area misfit
Layer thickness (Å)	d_{111} = 2.968	d_{101} = 3.133	+5.57	Good compatibility for 2D absorption

Table ESI_1a: The alternative coincidence cell between NaF and formamide

	NaF {111}	**formamide {101}**		Notes
2D-cell vectors	$[0\bar{2}2]$ = 13.106 $[3\bar{2}\bar{1}]$ = 17.338	$[1\bar{1}\bar{1}]$= 12.297 $[21\bar{2}]$= 18.633	–6.58 +7.47	Low and opposite linear misfits
2D-cell Area	223.132	224.706	**+ 0.70**	Very low area misfit and multiplicity = 6× NaF {111}unit cell

Table ESI_2. The coincidence lattices between formamide and the alkali halides in the "NaCl mode" (a comparison between *LiCl, KF, LiBr, NaCl, RbF, NaBr, CsF, LiI* and *KCl*)

	Host crystal	**Guest crystal**	**Misfit *m* (%)**	**Notes**
	LiCl {111}	**formamide {101}**		
2D-cell vectors	$2\times[11\bar{2}]$= 25.181 $[1\bar{1}0]$= 7.269	3×[010]= 27.802 $[10\bar{1}]$= 8.083	+ 10.41 +11.20	Medium-high linear misfits
2D-cell Area	**183.037**	224.723	**+22.77**	Very high area misfit
Layer thickness (Å)	2.967	d_{101} = 3.133	+5.57	Good compatibility for 2D absorption
	KF {111}	**formamide {101}**		
2D-cell vectors	$2\times[11\bar{2}]$= 26.192	3×[010]= 27.802	+ 6.146	Low and cooperating linear misfits

	$[1\bar{1}0]$= 7.561	$[10\bar{1}]$= 8.083	+6.904	
2D-cell Area	**198.038**	224.723	**+13.47**	Medium-high area misfit
Layer thickness (Å)	d_{111} = 3.087	d_{101} = 3.133	+1.49	Very good compatibility for 2D absorption
	LiBr {111}	**formamide {101}**		
2D-cell vectors	$2\times[11\bar{2}]$= 26.947 $[1\bar{1}0]$= 7.779	$3\times[010]$= 27.802 $[10\bar{1}]$= 8.083	+ 3.172 +3.907	Low and cooperating linear misfits
2D-cell Area	**209.622**	224.723	**+7.204**	Low area misfit
Layer thickness (Å)	d_{111} = 3.176	d_{101} = 3.133	– 1.37	Very good compatibility for 2D absorption
	NaCl {111}	**formamide {101}**		
2D-cell vectors	$2\times[11\bar{2}]$= 27.632 $[1\bar{1}0]$= 7.976	$3\times[010]$= 27.802 $[10\bar{1}]$= 8.083	+ 0.62 +1.68	Very low and cooperating linear misfits
2D-cell Area	220.393	224.723	**+ 1.96**	Very low area misfit
Layer thickness (Å)	d_{111} = 3.256	d_{101} = 3.133	– 3.92	Very good compatibility for 2D absorption
	RbF {111}	**formamide {101}**		
2D-cell vectors	$2\times[11\bar{2}]$= 27.688 $[1\bar{1}0]$= 7.993	$3\times[010]$= 27.802 $[10\bar{1}]$= 8.083	+ 0.41 +1.126	Very low and cooperating linear misfits
2D-cell Area	221.314	224.723	**+1.538**	Very low area misfit
Layer thickness (Å)	d_{111} = 3.263	d_{101} = 3.133	– 3.99	Very good compatibility for 2D absorption
	NaBr {111}	**formamide {101}**		
2D-cell vectors	$2\times[11\bar{2}]$= 29.282 $[1\bar{1}0]$= 8.453	$3\times[010]$= 27.802 $[10\bar{1}]$= 8.083	–5.32 –4.58	Low and cooperating linear misfits
2D-cell Area	247.52	224.723	**– 10.14**	Medium-high area misfit
Layer thickness (Å)	d_{111} = 3.451	d_{101} = 3.133	– 10.15	Very low compatibility for 2D absorption
	CsF {111}	**formamide {101}**		
2D-cell vectors	$2\times[11\bar{2}]$= 29.462 $[1\bar{1}0]$= 8.505	$3\times[010]$= 27.802 $[10\bar{1}]$= 8.083	– 5.97 – 5.22	Low and cooperating linear misfits
2D-cell Area	250.574	224.723	**– 11.51**	Medium-high area misfit

Layer thickness (Å)	d_{111} = 3.472	d_{101} = 3.133	– 10.82	Very low compatibility for 2D absorption
	LiI {111}	**formamide {101}**		
2D-cell vectors	$2\times[11\bar{2}]$= 29.5072 $[1\bar{1}0]$= 8.518	3×[010]= 27.802 $[10\bar{1}]$= 8.083	– 6.13 – 5.38	Low and cooperating linear misfits
2D-cell Area	251.342	224.723	**– 12.04**	Medium-high area misfit
Layer thickness (Å)	d_{111} = 3.477	d_{101} = 3.133	– 10.99	Very low compatibility for 2D absorption
	KCl {111}	**formamide {101}**		
2D-cell vectors	$2\times[11\bar{2}]$= 30.827 $[1\bar{1}0]$= 8.899	3×[010]= 27.802 $[10\bar{1}]$= 8.083	– 10.88 – 10.09	Medium-high and cooperating linear misfits
2D-cell Area	251.342	224.723	**– 22.10**	High area misfit
Layer thickness (Å)	d_{111} = 3.633	d_{101} = 3.133	– 15.96	Very low compatibility for 2D absorption

Table ESI_3. The coincidence lattices between formamide and the alkali halides in the "KBr mode" (a comparison between *LiI, KCl, NaI, RbCl, KBr, RbBr, KI* and *RbI*)

	Host crystal	**Guest crystal**	**Misfit *m* (%)**	**Notes**
	LiI {111}	**formamide {101}**		
2D-cell vectors (Å)	$[11\bar{2}]$ = 14.7536 $[1\bar{1}0]$ = 8.518	$2\times[10\bar{1}]$ = 16.165 [010] = 9.267	+9.566 +8.795	Low-medium and cooperating linear misfits
2D-cell area (Å²)	125.671	149.801	**+19.20**	Very high area misfit
Layer thickness (Å)	d_{111} = 3.477	d_{101} = 3.133	10.99	Very low compatibility for 2D absorption
	KCl {111}	**formamide {101}**		
2D-cell vectors (Å)	$[11\bar{2}]$ = 15.4135 $[1\bar{1}0]$ = 8.899	$2\times[10\bar{1}]$ = 16.165 [010] = 9.267	+4.875 +4.137	Low and cooperating linear misfits
2D-cell area (Å²)	137.165	149.801	+9.212	Low-Medium area misfit
Layer thickness (Å)	$5\times d_{111}$ = 18.166	$6\times d_{101}$ = 18.798	3.48	Low compatibility for 2D absorption
	NaI {111}	**formamide {101}**		
2D-cell vectors (Å)	$[11\bar{2}]$ = 15.855	$2\times[10\bar{1}]$ = 16.165	+1.95	Low and cooperating linear misfits

	$[1\bar{1}0] = 9.154$	[010] = 9.267	+1.237	
2D-cell area (Å²)	145.138	149.801	**+3.21**	Low area misfit
Layer thickness (Å)	$4\times d_{111} = 14.948$	$5\times d_{101} = 15.665$	4.80	Medium-low compatibility for 2D absorption
	RbCl {111}	**formamide {101}**		
2D-cell vectors (Å)	$[11\bar{2}] = 16.120$ $[1\bar{1}0] = 9.307$	$2\times[10\bar{1}] = 16.165$ [010] = 9.267	+ 0.28 – 0.429	Very low and opposite linear misfits
2D-cell area (Å²)	150.031	149.801	**– 0.151**	Very low area misfit
Layer thickness (Å)	$4\times d_{111} = 15.198$	$5\times d_{101} = 15.665$	3.07	Low compatibility for 2D
	KBr {111}	**formamide {101}**		
2D-cell vectors (Å)	$[11\bar{2}] = 16.167$ $[1\bar{1}0] = 9.334$	$2\times[10\bar{1}] = 16.165$ [010] = 9.267	– 0.012 – 0.723	Very low and cooperating linear misfits
2D-cell area (Å²)	150.902	149.801	**– 0.735**	Very low 2D cell multiplicity
Layer thickness (Å)	$4\times d_{111} = 15.24$	$5\times d_{101} = 15.665$	2.79	Low compatibility for 2D absorption
	RbBr {111}	**formamide {101}**		
2D-cell vectors (Å)	$[11\bar{2}] = 16.8736$ $[1\bar{1}0] = 9.742$	$2\times[10\bar{1}] = 16.165$ [010] = 9.267	– 4.38 – 5.12	Low-medium and cooperating linear misfits
2D-cell area (Å²)	164.383	149.801	**– 9.73**	Low-Medium area misfit
Layer thickness (Å)	$3\times d_{111} = 11.932$	$4\times d_{101} = 12.538$	5.08	Medium-low compatibility for 2D absorption
	KI {111}	**formamide {101}**		
2D-cell vectors (Å)	$[11\bar{2}] = 17.308$ $[1\bar{1}0] = 9.993$	$2\times[10\bar{1}] = 16.165$ [010] = 9.267	– 7.07 – 7.83	Low-medium and cooperating linear misfits
2D-cell area (Å²)	172.962	149.801	**– 15.46**	High area misfit
Layer thickness (Å)	$3\times d_{111} = 12.238$	$4\times d_{101} = 12.538$	2.44	Medium compatibility for 2D absorption
	RbI {111}	**formamide {101}**		
2D-cell vectors (Å)	$[11\bar{2}] = 17.984$ $[1\bar{1}0] = 10.383$	$2\times[10\bar{1}] = 16.165$ [010] = 9.267	– 11.25 – 12.04	High and cooperating linear misfit
2D-cell area (Å²)	186.728	149.801	**– 24.65**	Very high area misfit
Layer thickness (Å)	$3\times d_{111} = 12.716$	$4\times d_{101} = 12.538$	1.42	Medium compatibility for

				2D absorption

Table ESI_4. The coincidence lattices between the alkali halides and the hexagonal Ice (Ih) in the "NaF mode" (a comparison between *LiF, NaF* and *LiCl*)

	Host crystal	**Guest crystal**	**Misfit** ***m*** **(%)**	
	LiF {111}	**hexagonal Ice (I_h) {00.1}**		
2D-cell vectors	$2 \times [10\bar{1}] = 11.39$ $2 \times [\bar{1}10] = 11.39$	$3 \times [100] = 13.539$ $3 \times [010] = 13.539$	+18.87 +18.87	Very high and cooperating linear misfit
2D-cell Area	112.35	158.746	**+ 41.29**	Very high area misfit
Layer thickness (Å)	$3 \times d_{111} = 6.975$	$2 \times d_{00.1} = 7.356$	5.46	Good compatibility for 2D absorption
	NaF {111}	**hexagonal Ice (I_h) {00.1}**		**Notes**
2D-cell vectors	$2 \times [10\bar{1}] = 13.106$ $2 \times [\bar{1}10] = 13.106$	$3 \times [100] = 13.539$ $3 \times [010] = 13.539$	+3.30 +3.30	Low and cooperating linear misfits
2D-cell Area	148.754	158.746	+ 6.72	Low area misfit
Layer thickness (Å)	$3 \times d_{111} = 6.683$	$2 \times d_{00.1} = 7.356$	+ 10.07	Very low compatibility for 2D absorption
	LiCl {111}	**hexagonal Ice (I_h) {00.1}**		
2D-cell vectors	$2 \times [10\bar{1}] = 14.538$ $2 \times [\bar{1}10] = 14.538$	$3 \times [100] = 13.539$ $3 \times [010] = 13.539$	–7.38 –7.38	Low-medium and cooperating linear misfits
2D-cell Area	183.037	158.746	**– 15.30**	High area misfit
Layer thickness (Å)	$5 \times d_{111} = 14.838$	$4 \times d_{00.1} = 14.712$	0.85	Low-medium compatibility for 2D absorption

Table ESI_5. The coincidence lattices between the alkali halides and the hexagonal Ice (Ih) in the "LiBr mode" (a comparison between:*LiCl, KF, LiBr, NaCl, RbF, NaBr, CsF* and *LiI*).

	Host crystal	Guest crystal	Misfit *m* (%)	Notes
2D-cell vectors	**LiCl {111}**	**hexagonal Ice (I_h) {00.1}**		
2D-cell Area	$[\bar{1}10]$= 7.269 $[10\bar{1}]$ = 7.269	$[\bar{1}10]$= 7.817 [210]= 7.817	+7.54 +7.54	Medium-low and cooperating linear misfits
Layer thickness (Å)	45.759	52.919	**+ 15.64**	High area misfit
	$5\times d_{111}$ = 14.84	$4\times d_{00.2}$ = 14.71	**0.88**	Low compatibility for 2D absorption
	KF {111}	**hexagonal Ice (I_h) {00.1}**		
2D-cell vectors	$[\bar{1}10]$= 7.5618 $[10\bar{1}]$ = 7.5618	$[\bar{1}10]$= 7.817 [210]= 7.817	+3.37 +3.37	Low and cooperating linear misfits
2D-cell Area	49.520	52.919	**+ 6.86**	Low area misfit
Layer thickness (Å)	$6\times d_{111}$ = 18.52	$5\times d_{00.2}$ = 18.38	0.72	Very low compatibility for 2D absorption
	LiBr {111}	**hexagonal Ice (I_h) {00.1}**		
2D-cell vectors	$[\bar{1}10]$= 7.779 $[10\bar{1}]$ = 7.779	$[\bar{1}10]$= 7.817 [210]= 7.817	+0.48 +0.48	Very low and cooperating linear misfits
2D-cell Area	52.413	52.919	**+ 0.96**	Very low area misfit
Layer thickness (Å)	d_{111} = 3.176	$d_{00.2}$ = 3.677	15.77	No compatibility for 2D absorption
	NaCl {111}	**hexagonal Ice (I_h) {00.1}**		
2D-cell vectors	$[\bar{1}10]$= 7.976 $[10\bar{1}]$ = 7.976	$[\bar{1}10]$= 7.817 [210]= 7.817	–2.04 –2.04	Low and cooperating linear misfits
2D-cell Area	55.093	52.919	**–4.11**	Low area misfit
Layer thickness (Å)	$6\times d_{111}$ = 19.537	$5\times d_{00.2}$ = 18.38	6.25	Very low compatibility for 2D absorption
	RbF {111}	**hexagonal Ice (I_h) {00.1}**		
2D-cell vectors	$[\bar{1}10]$= 7.993 $[10\bar{1}]$ = 7.993	$[\bar{1}10]$= 7.817 [210]= 7.817	–2.25 –2.25	Low and cooperating linear misfits
2D-cell Area	55.328	52.919	**–4.55**	Low area misfit
Layer thickness (Å)	$6\times d_{111}$ = 19.579	$5\times d_{00.2}$ = 18.38	6.48	Very low compatibility for 2D absorption

	NaBr {111}	hexagonal Ice (I_h) {00.1}		
2D-cell vectors	$[\bar{1}10]$= 8.453 $[10\bar{1}]$ = 8.453	$[\bar{1}10]$= 7.817 [210]= 7.817	−8.13 −8.13	Medium and cooperating linear misfits
2D-cell Area	61.88	52.919	**−16.93**	High area misfit
Layer thickness (Å)	d_{111} = 3.451	$d_{00.2}$ = 3.677	6.56	Low-medium compatibility for 2D absorption
	CsF {111}	**hexagonal Ice (I_h) {00.1}**		
2D-cell vectors	$[\bar{1}10]$= 8.505 $[10\bar{1}]$ = 8.505	$[\bar{1}10]$= 7.817 [210]= 7.817	−8.80 −8.80	Medium and cooperating linear misfits
2D-cell Area	62.44	52.919	**−18.38**	High area misfit
Layer thickness (Å)	d_{111} = 3.472	$d_{00.2}$ = 3.677	5.90	Low-medium compatibility for 2D absorption
	LiI {111}	**hexagonal Ice (I_h) {00.1}**		
2D-cell vectors	$[\bar{1}10]$= 8.518 $[10\bar{1}]$ = 8.518	$[\bar{1}10]$= 7.817 [210]= 7.817	−8.96 −8.96	Medium and cooperating linear misfits
2D-cell Area	62.835	52.919	**−18.74**	High area misfit
Layer thickness (Å)	d_{111} = 3.477	$d_{00.2}$ = 3.677	5.74	Low-medium compatibility for 2D absorption

Table ESI_6. The coincidence lattices between the alkali halides and the hexagonal Ice (Ih) in the "KCl mode" (a comparison between*: LiI, KCl, NaI, RbCl, KBr, RbBr, KI* and *RbI*).

	Host crystal	Guest crystal	Misfit *m* (%)	Notes
	LiI {111}	**hexagonal Ice (I_h) {00.1}**		
2D-cell vectors	$[\bar{1}10]$= 8.518 $[10\bar{1}]$ = 8.518	[020]= 9.026 [200]= 9.026	+5.966 +5.966	Low and cooperating linear misfits
2D-cell Area	62.835	70.554	**+ 12.28**	High area misfit
Layer thickness (Å)	$5\times d_{111}$ = 14.84	$4\times d_{00.2}$ = 14.71	0.88	Low compatibility for 2D absorption
	KCl {111}	**hexagonal Ice (I_h) {00.1}**		
2D-cell vectors	$[\bar{1}10]$= 8.899	[020]= 9.026	+1.42	Low and cooperating linear

	$[10\bar{1}] = 8.899$	[200]= 9.026	+1.42	misfits
2D-cell Area	68.582	70.554	**+ 2.87**	Low area misfit
Layer thickness (Å)	$d_{111} = 3.633$	$d_{00.2} = 3.677$	1.20	Very good compatibility for 2D absorption
	NaI {111}	**hexagonal Ice (I_h) {00.1}**		
2D-cell vectors	$[\bar{1}10]= 9.154$ $[10\bar{1}] = 9.154$	[020]= 9.026 [200]= 9.026	–1.42 –1.42	Low and cooperating linear misfits
2D-cell Area	72.569	70.554	**– 2.85**	Low area misfit
Layer thickness (Å)	$d_{111} = 3.737$	$d_{00.2} = 3.677$	1.63	Very good compatibility for 2D absorption
	RbCl {111}	**hexagonal Ice (I_h) {00.1}**		
2D-cell vectors	$[\bar{1}10]= 9.307$ $[10\bar{1}] = 9.307$	[020]= 9.026 [200]= 9.026	–3.11 –3.11	Low and cooperating linear misfits
2D-cell Area	75.015	70.554	**– 6.32**	Low-medium area misfit
Layer thickness (Å)	$d_{111} = 3.799$	$d_{00.2} = 3.677$	3.32	Very good compatibility for 2D absorption
	KBr {111}	**hexagonal Ice (I_h) {00.1}**		
2D-cell vectors	$[\bar{1}10]= 9.334$ $[10\bar{1}] = 9.334$	[020]= 9.026 [200]= 9.026	–3.41 –3.41	Low and cooperating linear misfits
2D-cell Area	75.451	70.554	**– 6.94**	Low-medium area misfit
Layer thickness (Å)	$d_{111} = 3.810$	$d_{00.2} = 3.677$	3.63	Very good compatibility for 2D absorption
	KBr {111}	**hexagonal Ice (I_h) {00.1}**		
2D-cell vectors	$[\bar{1}10]= 9.742$ $[10\bar{1}] = 9.742$	[020]= 9.026 [200]= 9.026	–7.94 –7.94	Low-medium and cooperating linear misfits
2D-cell Area	82.191	70.554	**– 16.49**	High area misfit
Layer thickness (Å)	$d_{111} = 3.977$	$d_{00.2} = 3.677$	8.14	Low compatibility for 2D absorption
	KI {111}	**hexagonal Ice (I_h) {00.1}**		
2D-cell vectors	$[\bar{1}10]= 9.993$ $[10\bar{1}] = 9.993$	[020]= 9.026 [200]= 9.026	–10.71 –10.71	Medium-high and cooperating linear misfits
2D-cell Area	86.481	70.554	**– 22.57**	Very high area misfit
Layer thickness	$d_{111} = 4.079$	$d_{00.2} = 3.677$	10.93	Very low compatibility for

(Å)				2D absorption
	RbI {111}	**hexagonal Ice (I_h) {00.1}**		
2D-cell vectors	$[\bar{1}10]$= 10.383 $[10\bar{1}]$ = 10.383	[020]= 9.026 [200]= 9.026	–15.03 –15.03	Very high and cooperating linear misfits
2D-cell Area	93.363	70.554	**– 32.32**	Very high area misfit
Layer thickness (Å)	$5\times d_{111}$ = 21.195	$6\times d_{00.2}$ = 22.065	4.10	Low compatibility for 2D absorption